AD-A128 239 ELECTRON AND PHOTON STIMULATED DESORPTION: BENEFITS AND 1/1
PITFALLS(U) NATIONAL BUREAU OF STANDARDS WASHINGTON DC
SURFACE SCIENCE DIV T E MADEY ET AL. 01 MAY 83 TR-33
UNCLASSIFIED N00014-83-F-0002 F/G 7/4 NL

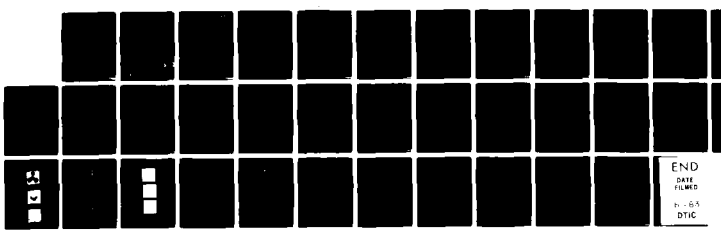

END
DATE FILMED
DTIC

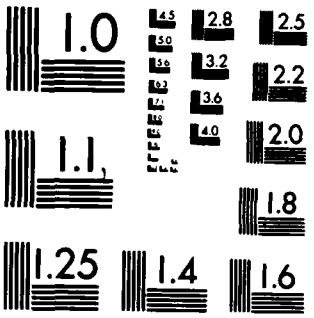

MICROCOPY RESOLUTION TEST CHART
NATIONAL BUREAU OF STANDARDS-1963-A

OFFICE OF NAVAL RESEARCH

Contract N00014-83-F-0002

TECHNICAL REPORT NO. 33

ELECTRON AND PHOTON STIMULATED DESORPTION: BENEFITS AND PITFALLS

by

Theodore E. Madey, D.L. Doering, E. Bertel and R. Stockbauer
Surface Science Division
National Bureau of Standards
Washington, DC 20234

May 1, 1983

To appear in Ultramicroscopy

SECURITY CLASSIFICATION OF THIS PAGE (When Data Entered)

REPORT DOCUMENTATION PAGE	READ INSTRUCTIONS BEFORE COMPLETING FORM
1. REPORT NUMBER: Technical Report No. 33 — 2. GOVT ACCESSION NO.: AD-A128239	3. RECIPIENT'S CATALOG NUMBER
4. TITLE (and Subtitle): Electron and Photon Stimulated Desorption: Benefits and Pitfalls	5. TYPE OF REPORT & PERIOD COVERED: Interim
	6. PERFORMING ORG. REPORT NUMBER
7. AUTHOR(s): Theodore E. Madey, D.L. Doering, E. Bertel and R. Stockbauer	8. CONTRACT OR GRANT NUMBER(s): N00014-83-F-0002
9. PERFORMING ORGANIZATION NAME AND ADDRESS: Surface Science Division, National Bureau of Standards, Washington, DC 20234	10. PROGRAM ELEMENT, PROJECT, TASK AREA & WORK UNIT NUMBERS
11. CONTROLLING OFFICE NAME AND ADDRESS: Office of Naval Research, Physical Science Program Office, Arlington, VA 22217	12. REPORT DATE: May 1, 1983
	13. NUMBER OF PAGES: 33
14. MONITORING AGENCY NAME & ADDRESS(if different from Controlling Office)	15. SECURITY CLASS. (of this report): Unclassified
	15a. DECLASSIFICATION/DOWNGRADING SCHEDULE

16. DISTRIBUTION STATEMENT (of this Report)

Approved for public release; Distribution unlimited

17. DISTRIBUTION STATEMENT (of the abstract entered in Block 20, if different from Report)

18. SUPPLEMENTARY NOTES

To be published in Ultramicroscopy

19. KEY WORDS (Continue on reverse side if necessary and identify by block number)

chemisorption; electron beam damage; electron stimulated desorption; nickel; photon stimulated desorption; ruthenium; surface chemistry; water

20. ABSTRACT (Continue on reverse side if necessary and identify by block number)

Electron beam irradiation of solids often results in damage-producing events along with information-producing events. In the present paper we explore mechanisms of beam damage in solids, as well as examples of the benefits of electron (and photon) stimulated processes to study molecules at surfaces. Information about the geometrical structure of adsorbed species can be obtained from measurements of the angular distribution of ions released by electron or photon stimulated desorption. The directions of ion emission are

DD FORM 1 JAN 73 1473 EDITION OF 1 NOV 65 IS OBSOLETE

S/N 0102-LF-014-6601

SECURITY CLASSIFICATION OF THIS PAGE (When Data Entered)

Block 20 Continued

directly related to the orientations of the surface bonds which are ruptured by the excitation. The method of Electron Stimulated Desorption Ion Angular Distributions (ESDIAD) has proven particularly useful in characterizing local molecular structure at surfaces in the absence of long range order; recent measurements of bonding configurations stabilized by impurities or by lateral interactions are discussed. Photon stimulated desorption (PSD) studies using synchrotron radiation are providing new insights into fundamental electronic excitation processes at surfaces. Mechanisms for the excitation and desorption of ions are examined (valence, shallow core level and deep core level excitations), and examples include ion desorption from adsorbed monolayers, as well as ion formation and desorption processes in condensed molecular films.

Electron and Photon Stimulated Desorption: Benefits and Pitfalls

Theodore E. Madey, D.L. Doering,* E. Bertel**
and R. Stockbauer
Surface Science Division
National Bureau of Standards
Washington, DC 20234 USA

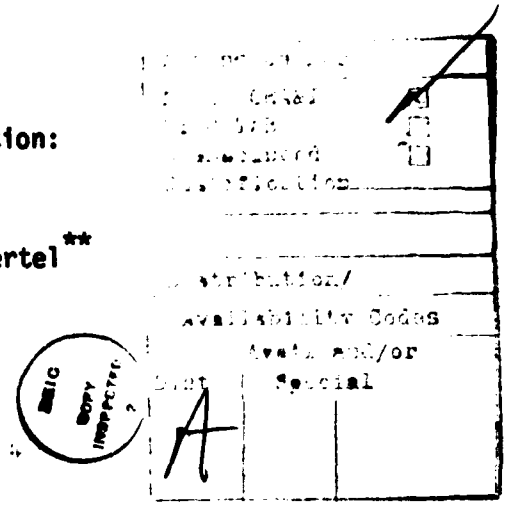

Abstract

Electron beam irradiation of solids often results in damage-producing events along with information-producing events. In the present paper we explore mechanisms of beam damage in solids, as well as examples of the benefits of electron (and photon) stimulated processes to study molecules at surfaces. Information about the geometrical structure of adsorbed species can be obtained from measurements of the angular distribution of ions released by electron or photon stimulated desorption. The directions of ion emission are directly related to the orientations of the surface bonds which are ruptured by the excitation. The method of Electron Stimulated Desorption Ion Angular Distributions (ESDIAD) has proven particularly useful in characterizing local molecular structure at surfaces in the absence of long range order; recent measurements of bonding configurations stabilized by impurities or by lateral interactions are discussed. Photon stimulated desorption (PSD) studies using synchrotron radiation are providing new insights into fundamental electronic excitation processes at surfaces. Mechanisms for the excitation and desorption of ions are examined (valence, shallow core level and deep core level excitations), and examples include ion desorption from adsorbed monolayers, as well as ion formation and desorption processes in condensed molecular films.

* NBS/NRC Postdoctoral Research Associate

** NBS Visiting Scientist, and Visiting Professor, Dept. of Physics, U. of Maryland. Permanent Address: Institute of Physical Chemistry, University of Innsbruck, Innsbruck, Austria.

I. Introduction

The electron and photon stimulated desorption (ESD/PSD) of ions and neutrals from surfaces has been shown to be a sensitive probe of structure and bonding for molecules adsorbed on surfaces [1-3]. The yields of ions and neutrals are sensitive to the binding sites of molecules on surfaces [1,2] and the ESD ion angular distributions (ESDIAD) provide direct information about the orientation of surface bonds [3,4]. Moreover, there is a clear relationship between ESD/PSD phenomena and beam damage processes in electron microscopy, so that these are fitting topics for a workshop on high resolution electron microscopy. In general, energetic electron or photon beams (10 eV to > 1000 eV) interacting with solids can cause electronic excitations at the surface and in the bulk which, if they remain localized long enough to produce atomic or ionic motion, can result in "beam damage": dissociation, diffusion, ion-molecule reactions, desorption, etc. [5]. In the present work, we will concentrate on those electron- and photon-induced electronic excitations occurring near or in the top monolayer of a solid which lead to desorption of ions, neutrals or metastables from the surface.

For electron microscopists, ESD/PSD phenomena are nuisances which should be avoided, or at least, be understood and controlled. For surface scientists, ESD/PSD can provide new insights into structure and bonding of surface molecules. In this paper, we will discuss the utility of ESD in surface science, as well as the mechanisms of ESD/PSD processes which can lead to a better understanding of beam damage in electron microscopy.

During the last few years, one of the main benefits of ESD has been the use of the ESD ion angular distribution (ESDIAD) method and the angle resolved PSD method for determining surface molecular structure [1,3,4]. In these methods, electronic excitation of surface molecules by a focused electron or photon beam can result in desorption of atomic and/or molecular

ions from the surface. The ions are found to desorb in discrete cones of emission in directions determined by the orientation of the bonds which are ruptured by the excitation. For example, as illustrated in Fig. 1, ESD or PSD of CO bound in an upright configuration on a metal surface will result in desorption of O^+ in the direction of the surface normal; "inclined" CO will produce ions in an off-normal direction. ESD/PSD of H^+ from H_2O bound to the surface via the O atom will result in desorption of H^+ in an off-normal direction. Measurements of the patterns of ion desorption provide a direct display of the geometrical structure of surface molecules in the adsorbed layer. In the following sections, several examples of the use of ESDIAD to determine the bonding geometry of adsorbed molecules will be presented.

In most cases, the electronic excitations which cause desorption of surface species can be initiated by either electron or photon bombardment. However, the excitation threshold energies for dipole-allowed transitions are sharper using photons, so that PSD studies performed using synchrotron radiation are particularly useful in clarifying the specific excitations which lead to desorption. The use of both ESD and PSD for identifying different desorption mechanisms will be explored in detail below.

The plan of the present paper is as follows: Section II contains a brief description of experimental procedures, and the application of ESDIAD to specific systems is described in Section III. Examples include several instances of short-range ordering effects induced in adsorbed molecules by surface impurities. Section IV contains a discussion of the electronic excitation mechanisms which lead to desorption, including core and valence excitation in both covalent and ionically-bonded systems. Conclusions and future directions are outlined in Section V.

Several reviews and anthologies of ESD/PSD have appeared recently, and the interested reader is referred to these papers [1-8].

II. Experimental Procedures

Extensive discussions of experimental methods in ESD and PSD have been given previously [1,3,6,9], and these will not be considered in detail again here.

Two types of ion detectors have been used for most of the published ESDIAD studies: an area detector with a visual display, and a scanning ion detector. In the display-type apparatus used at NBS [3,6] a focused electron beam (75-1500 eV) bombards a single crystal sample. The beams of ions which desorb via ESD pass through high-transparency hemispherical grids, and impinge on the front surface of a double microchannel plate (MCP) assembly. The output secondary electron signal from the MCP assembly is accelerated to a fluorescent screen where it is displayed visually (the ESDIAD pattern) and photographed. By changing potentials, the elastic low energy electron diffraction (LEED) pattern from the sample can also be studied. Ion masses are determined using a quadrupole mass spectrometer. Niehus [4,10] uses a channeltron electron multiplier mounted on a computer-driven gonimometer as a moveable ion detector for ESDIAD. His data are displayed as computer-generated plots of ion intensity vs. desorption angle; ion mass is determined using a time-of-flight method.

There have been few direct measurements of ESD neutral species. Feulner, Treichler and Menzel [11] have used an improved mass spectrometric method for detecting low-level neutral signals at or near the thresholds for desorption.

In PSD studies using synchrotron radiation, the relatively low ion signals and high background signals from scattered light introduce particular problems for angle-resolved measurements. A display-type ellipsoidal mirror analyzer has been used for several angle resolved PSD studies [12-14], but most PSD measurements to date are not angle resolved. Knotek and colleagues

have used a simple time-of-flight ion detector [15] for PSD; the NBS and Bell Laboratories groups have used a double pass cylindrical mirror analyzer for both mass and energy analysis of ESD/PSD ions [9,16,17].

III. Electron Stimulated Desorption Ion Angular Distributions (ESDIAD): *Relation to Surface Structure*

(a) Experimental basis of ESDIAD

During the last few years, it has become well-established that the directions of desorption of ESD ions are related to the orientations of the bonds ruptured by the electronic excitations, and that the ESDIAD method provides direct information about the structures of surface molecules [3,4,6]. The main foundation for this relation has been experimental. To "calibrate" the method, ESDIAD has been applied to a number of adsorbate-substrate systems whose surface geometries had already been predicted or determined using other structure-sensitive surface probes. In each case which has been studied to date, the ESDIAD results are consistent with the other techniques. For example, for standing-up CO on Ru(001) and Ni(111), the molecule is known to be bound via the carbon atom to the metal surface with its molecular axis perpendicular to the surface; ESD O^+ (and CO^+) ions desorb in the direction perpendicular to the surface [18,19]. For "inclined" CO on Pd(210), ESD of O^+ occurs in the predicted off-normal direction. For a number of additional systems [20], including NH_3 on Ru(001) and Ni(111), NO on Ni(111) and C_6H_{12} on Ru(001), the structural assignments based on ESDIAD measurements are consistent with bonding geometries determined using other surface methods.

For all adsorbed molecular systems where confirmatory evidence of surface structure is available, the ion desorption angle observed in ESDIAD is related to the surface bond angle. In particular, the predicted azimuthal angle of the surface bond is preserved in ESDIAD, but the polar

angle is always increased for the ion trajectory, due to image charge effects [3,21]. The theoretical picture is less clear. Although several model calculations exist [22], there is no general theory of ESD angular distributions applicable to a wide class of systems.

(b) Application of ESDIAD to short-range local ordering in adsorbed H_2O

There is an important area in which ESDIAD has provided new information about the structures of surface molecules-information not readily obtainable using other available techniques. It was found by Netzer and Madey [23] that traces of preadsorbed oxygen on various surfaces will induce a high degree of azimuthal order in adsorbed molecules which are disordered azimuthally on the clean surface. This surprising oxygen-stabilized azimuthal-ordering effect has been studied for H_2O and NH_3 on Ni(111) [23-25] Al(111) [25] and Ru(001) [26].

In the following paragraphs, we give two examples of impurity-stablized structures: the stabilization of adsorbed molecular H_2O by an electronegative species - oxygen on Ni(111)-and by an electropositive species - Na on Ru(001). Such studies of H_2O adsorption are of direct relevance to fundamental investigations of electrochemical processes at electrode surfaces [27].

Fig. 2 is taken from Ref. 24 and contains a sequence of LEED and ESDIAD patterns for the adsorption of H_2O on clean and oxygen-dosed Ni(111). Fig. 2a is a LEED pattern from the clean surface, and Fig. 3b is an ESDIAD pattern characteristic of adsorbed H_2O on Ni(111) at 80 K, for coverages less than saturation of the chemisorbed H_2O layer bonded directly to the Ni(111). The center of the pattern is dim, with most of the H^+ ion emission directed away from the normal. This pattern is consistent with bonding of H_2O to Ni(111) via the O atom, with H atoms oriented away from the surface. This pattern indicates that the array of hydrogen-bonded H_2O molecules contains

a distribution of "tilt" angles measured with respect to the surface normal, as well as random distribution of azimuthal angles.

In contrast, the adsorption of low coverages of H_2O and 80 K onto the oxygen pre-dosed and annealed Ni(111) surface produces a highly-ordered three-fold ESDIAD pattern (Fig. 2c) with intense ion emission along [$\bar{1}\bar{1}$2] azimuths. Even at the lowest oxygen coverages used in this study ($\theta_O \lesssim 0.03$ monolayers), evidence for this oxygen-induced azimuthal ordering was found.

In Fig. 3, a structural model is proposed [23,24]. From LEED, it is known that oxygen is adsorbed in three-fold hollow sites on Ni(111). For H_2O bonded in atop sites as shown, the surface O--O distance for O-H_2O is 2.87 Å, as compared with the 2.75-2.96 Å range seen for the O--O distance in hydrogen-bonded ice. We assume that the strength of the (hydrogen-bonding) H_2O-O interaction is sufficient to overcome the H_2O-H_2O interactions, and orient the molecules on the surface. In this model the non-hydrogen-bonded ligands in Fig. 3 are the ones which are seen in the three-fold ESDIAD pattern. Either the hydrogen-bonded ligands are more effectively neutralized following electronic excitation, and are less likely to desorb as ions, or the H^+ ions from the hydrogen-bonded ligands follow shallow trajectories and are recaptured by the surface [3,21].

Fig. 4 contains a sequence of ESDIAD patterns demonstrating the influence of preadsorbed electropositive atoms, Na, on the structure of H_2O on Ru(001) [28]. Fig. 4a shows a "halo" of H^+ ion emission characteristic of H_2O monomers adsorbed on Ru(001) at 80 K for H_2O coverages $\lesssim 0.1$ monolayers. The H_2O molecules are bonded to Ru via the O atoms, with H ligands oriented away from the surface in a random azimuthal array. (At higher coverages, the adsorbed H_2O molecules interact with their neighbors via hydrogen bonds, and the formation of clusters of H_2O in registry with the Ru(001) substrate is observed [29]. The present discussion is limited

to low H_2O coverages).

When low coverages of H_2O ($\lesssim$ 0.1 monolayers) are dosed onto the Ru(001) surface precovered with a small amount of partially-ionically-bonded sodium ($\lesssim$ 0.1 monolayers), the bright halo-like ESDIAD pattern of Fig. 4b results. The intensity of H^+ emission in Fig. 4b is increased over that of Fig. 4a by a factor of 10^2 to 10^3! We believe that the presence of Na leads to a reorientation of the molecular H_2O into a configuration from which ion desorption is more favorable than from the clean Ru(001) surface: either neutralization is suppressed, or there is a reduced probability of H^+ recapture due to the image force. When the surface of Fig. 4b is heated to 200 K, the H_2O and Na both become highly mobile, and an ordered hexagon H^+ ESDIAD pattern (Fig. 4c) is observed as the sample is cooled to 80 K.

Fig. 5 shows a structural model which is consistent with the hexagon ESDIAD pattern of Fig. 4c. Na is believed to be adsorbed in three-fold hollow sites at low Na coverages [30], and we suggest that neighboring H_2O molecules are stabilized by the electrostatic interaction between the H_2O dipoles and the net positive charge on the adsorbed Na. In contrast to the H_2O + O/Ni(111), the H ligands are tilted <u>away</u> from the Na. Note that the structural model on the left side of Fig. 5 is consistent with a 3-beam ESDIAD pattern. The 6-beam hexagonal ESDIAD pattern is generated because structures similar to those of Fig. 5 are rotated by 60° upon crossing a monoatomic step on the hcp Ru(001) surface.

Side views of the proposed models of Fig. 3 and 5 for the adsorbed H_2O-O and H_2O-Na structures are shown in Fig. 6. These models of H_2O interacting with adsorbed electronegative and electropositive atoms are qualitatively consistent with the theoretical (Hartree-Fock) study of molecular complexes of H_2O with positive and negative ions ($Na^+ (H_2O)_n$, $Cl^- (H_2O)_n$, etc.) performed by Kistenmacher, Popkie and Clementi [31].

A striking result of this work is that for H_2O - anion interactions, the low energy configurations are ones in which the H_2O molecules are oriented with an OH bond in the direction of the anion. For H_2O - cation interactions, the H ligands are oriented away from the ion, and the structures can be described by point charge - dipole interactions. Other H_2O-cation structures are discussed in Ref. 28.

In closing this section, we emphasize that, in general, azimuthal ordering effects observed by ESDIAD are most pronounced for low coverages ($\lesssim$ 0.1 monolayer) of O or Na, and that higher coverages of the additive lead to disorder in the adsorbed H_2O as well as NH_3 [25,26]. The chemistry and binding energy of the adsorbates can also vary with coverage of the additive. For example, in the case of H_2O on a high coverage of Na, appreciable dissociation of H_2O occurs for $\Theta_{Na} \gtrsim 0.33$ monolayers [28].

In summary, some of the main advantages of ESDIAD for surface studies can be given as:

(1) ESDIAD provides direct information regarding surface structures: ion desorption angles are determined by surface bond angles

(2) ESDIAD is particularly sensitive to the orientation of H-ligands in adsorbed molecular complexes (low energy electron diffraction, LEED, is much less useful in this regard)

(3) ESDIAD is sensitive to the local bonding geometry in adsorbed molecular complexes; long range order is not necessary to produce an ordered ESDIAD pattern.

IV. Mechanisms of ESD/PSD Processes

A number of different initial electronic excitations have been identified as contributing to ESD and PSD of ions and neutrals from surfaces, including valence electron excitations, and both shallow and deep core hole excitations. It appears on the basis of evidence to date that ESD and PSD are initiated by the same elementary excitations, and that differences which occur in spectral yield curves (ion yield vs. energy of e^-, $h\nu$) reflect differences in the physics of the excitation process for electrons and photons. The different spectral dependences of ion desorption yields are described in detail by Knotek [32] and depend on a variety of factors (energy dependence of initial excitation cross section, final states accessible, and definition of energy deposition). In general, PSD ion yields rise sharply at threshold to a peak, and fall off at higher energy as $^1/E^n$, where $2 < n < 3$. ESD ion yields rise more slowly at threshold and reach broad peaks at 3-4 times the threshold energy. Hence, the relatively sharp PSD ion yields are generally more useful for isolating and identifying desorption mechanisms than are ESD yields. In the following paragraphs, we will explore ESD/PSD desorption mechanisms for several different classes of surface species: ionically-bonded surface atoms, covalently-bonded surface molecules, and condensed molecular films of covalently-bonded molecules.

(a) Ionic systems

Ion desorption from maximal valency, ionically-bonded surfaces is believed to proceed via an Auger decay mechanism proposed by Knotek and Feibelman (K-F) [33]. Maximal valency means that the cation is ionized down to the noble gas configuration (e.g., K^+, Ca^{2+}, Ti^{4+}, etc. in K_2O, CaO, TiO_2, etc.), and that the highest occupied level is its highest core level, of binding energy $\gtrsim$ 20 eV. There is always some degree of covalency, but to a first approximation, the valence electrons have little density at the

cation. In the K-F mechanism as applied to TiO_2, for example, ion desorption can be initiated by the production of a vacancy in the highest occupied core level, Ti 3p. The vacancy is filled by an interatomic Auger process involving an electron from the O^{2-}, and the release of two additional Auger electrons from the O^{2-} can leave the oxygen positively charged. The Coulomb potential for O^+ in the presence of Ti^{4+} is repulsive, and the O^+ will desorb from the surface.

An adsorbate system to which the KF mechanism appears applicable is the adsorption of oxygen on Ti(001), where a variety of evidence indicates that surface TiO_2 is formed [34]. Fig. 7 shows the PSD O^+ ion yield vs. photon energy, and compares it with the secondary electron yield from Ti, which is proportional to the Ti 3p ionization probability [35]. The similarity of the onsets and energy dependences of the O^+ ion yield and Ti 3p core hole excitation leads to the conclusion that ion desorption is initiated by the production of a Ti 3p core hole in accordance with the KF model. The differences in detail of the two curves of Fig. 7 may indicate additional excitation mechanisms also. Similar evidence for the KF process in ion desorption have been observed for W(111) [14], as well as a number of ionic solids [33].

(b) Covalent systems

The mechanisms for ion desorption from covalently-bonded systems are less characterized. The first ESD mechanism, proposed by Menzel, Gomer and Redhead [36,37], suggested a Franck-Condon type transition to a repulsive final state from which desorption or de-excitation (and possible recapture) could occur. The exact nature of the repulsive final states are just now being elucidated by theorists. In a number of cases, the most promising candidates are two-hole states in valence orbitals, in which the holes remain

localized on the surface molecule for a long enough period of time ($\sim 10^{-13}$ s) that bond rupture can occur and an ion can be ejected [38].

To illustrate PSD of a covalently-bonded adsorbate, CO on Ru(001) was studied [39]. CO is bonded in molecular form to Ru, via the carbon end of the molecule. The PSD O^+ ion yield as a function of photon energy is compared with the probability of Ru core level production in Fig. 8. There is little correlation between the onsets or structure in the two curves, indicating that Ru core levels are not involved in the ion desorption process in this energy range. Ramaker has recently proposed that the peak at 41 eV in Fig. 8 is due to a $5\sigma^{-2}\ 6\sigma^{2}$ excitation, and that the 50 eV peak is due to ionization of the CO 3σ state, which then undergoes heavy mixing with 2hle (two hole-one electron) states in the adsorbed molecule (40).

Feulner, Treichler and Menzel [11] and Jaeger et al [41] show that excitation of deep core levels (O1s, N1s, C1s) can also lead to desorption of ions from covalently-bonded adsorbates; a collection of their data [11] are shown in Fig. 9 for ESD of molecules adsorbed on metals. Adsorbate core hole ionization is quickly followed by Auger decay which ends in multiply valence-ionized adsorbate states. Certain of the "multiple-hole" states will lead to dissociation and desorption of ions.

(c) ESD/PSD of condensed films

We have used ESD/PSD techniques to study the electronic processes which lead to desorption of ions from condensed films of hydrogen-containing molecules, C_6H_{12} (cyclohexane), CH_3OH (methanol), and H_2O. In the condensed state, C_6H_{12} is bound primarily by van der Waals forces, whereas CH_3OH and H_2O are both hydrogen-bonded. We see striking differences in the mass distribution of ESD ions from these two classes of condensed films.

The dominant ESD ion from condensed layers of H_2O and CH_3OH is H^+, with yields of higher mass ions $\lesssim$ 2% of H^+. In addition, cluster ions

from the water film [$(H_2O)_nH^+$] were at the 0.1% level or less. The results are independent of film thickness. These observations are quantitatively different from the gas phase results, where high mass ions dominate in the mass spectra of both H_2O and CH_3OH.

Evidence for the mechanism of H^+ formation in condensed CH_3OH and H_2O comes from PSD in combination with ESD. PSD of ions from the condensed methanol has been studied over the photon energy range 15 to 75 eV, and the H^+ yield data are shown in Fig. 10. The threshold for H^+ desorption is at 18 eV, with the maximum yield at 25 eV [42]. This suggests that ionization of the 4a' level is the underlying mechanism, because its onset occurs near the 18 eV threshold. In order to determine if the H^+ desorption is due to C-H or O-H bond cleavage (or both), we studied low energy ESD of isotopically labelled CH_3OH films [43]. It was found that low-energy (<70 eV) electron excitation and fragmentation of CH_3OH results overwhelmingly in H^+ ejection by C-H bond cleavage. This is additional evidence for involvement of the 4a' level since it is dominantly a C-H bonding orbital. In contrast, the gas-phase fragmentation shows H^+ arising from both O-H and C-H bond cleavage [44].

PSD of H^+ from H_2O films (Fig. 10) has higher threshold and maximum yield energies than CH_3OH, and apparently arises from excitation of 2-hole valence states. Ramaker has identified specific two hole-one electron states ($1b_1^{-2}\ 4a_1$ and $1b_1^{-1}\ 3a_1^{-1}\ 4a_1$) as being responsible for H^+ desorption from H_2O films [45].

ESD of the non-hydrogen-bonded C_6H_{12} has been studied as a function of film thickness on a clean Cu(100) substrate using time of flight (TOF) mass spectrometry. For thin layers (corrected exposures $\lesssim$ 2.5 Langmuirs, where 1 Langmuir = 1L = 1 x 10^{-6} Torr sec) predominantly H^+ ions are seen. The H^+ ions have a most probable kinetic energy of 4 eV, and the H^+ yield

increases to a plateau value for exposures $\lesssim$ 4L (Fig. 11). For exposures $\gtrsim$ 2L, heavier ions appear in the ESD mass spectrum ($C_1H_n^+$,. . ., $C_6H_n^+$) having a most probable kinetic energy $\sim$ 2 eV (Fig. 12); the yield of heavy ions increases with both increasing film thickness and electron beam energy to > 150 eV. Beam damage (5) was negligible under conditions of these experiments. These results are qualitatively consistent with a model by which ions close to the metal surface are preferentially neutralized. The low kinetic energies and high masses of heavy fragments result in substantially lower velocities and, therefore, longer residence times near the metal surfaces than for H^+, so the heavy ions have a higher probability of reneutralization. The reneutralization rate decreases with increasing film thickness, causing an increased yield of higher mass fragments. The ESD ion mass spectrum from a thick layer of C_6H_{12} is qualitatively similar to the gas phase mass spectrum. As indicated above, ESD of hydrogen-bonded film of H_2O and CH_3OH yields primarily H^+, with only trace levels of high mass ions (Fig. 12).

The absence of heavy ion fragments in the ESD mass spectra of H_2O and CH_3OH films appears to be related to hydrogen-bonding in the condensed layers. Hydrogen-bonding may provide an effective de-excitation mechanism for heavy ion fragments, via a strong coupling between adjacent molecules through which the electronic or vibronic excitation becomes delocalized. The reduced yield of heavy ions may also be due to proton transfer reactions occurring at the surface of the film before or during desorption, a process which could effectively reneutralize the desorbed heavy ions. Hydrogen-bonding, however, is not significant in condensed C_6H_{12}, nor do proton transfer processes occur with high probability in ion-molecule collisions of C_6H_{12} and its fragments. Thus, in agreement with the proposed model, heavy ion fragments are not strongly suppressed in ESD of C_6H_{12}.

V. Summary and Conclusions

This paper has had a limited objective: to introduce electron microscopists to some of the benefits and pitfalls of electron and photon stimulated desorption. We have not emphasized the quantitative aspects of cross sections for electron- and photon-induced beam damage in different materials (cf. Ref. 5 for a discussion of this point), but have concentrated on a discussion of the physical mechanisms and applications of ESD/PSD.

One of the main benefits of ESD/PSD as applied to studies of surfaces is the fact that direct information concerning the structures of surface molecules can be obtained from measurements of ESD ion angular distributions (ESDIAD). The directions of ion emission in ESD or PSD are directly related to the orientations of the surface bonds which are ruptured by the excitations. Several examples where ESDIAD has been used to provide new information about the structures of adsorbed molecules were discussed.

The pitfalls of ESD/PSD processes are, of course, due to the fact that these are inherently destructive techniques: the surface bond is broken in order to perform the analysis of surface structure. However, by studying the threshold energies for desorption of ions, as well as the spectral dependence of ion desorption (ion yield vs. photon energy), information regarding the mechanisms of radiation damage by electrons and photons is obtained. Such studies have provided new insights into the electronic excitation mechanisms which can lead to "beam damage" in electron microscopy. Examples which were discussed included ion desorption due to excitation of valence levels in covalently-bonded molecules, shallow core levels in ionically-bonded species, and deep core levels.

In concluding, we note that most ESD/PSD studies which have been performed to date (and virtually all the examples discussed herein) have

concerned desorption of ions, because of their ease of detection. An important future challenge will be the characterization of desorption mechanisms and angular distributions of neutral species. In many cases, neutrals are the majority of desorbing species, and an understanding of neutral desorption should provide new insights into the mechanisms of radiation damage.

VI. Acknowledgements

This work was supported in part by the Department of Energy, Division of Basic Energy Sciences, and in part by the Office of Naval Research.

References

[1] See "Desorption Induced by Electronic Transitions", in N.H. Tolk, M.M. Traum, J.C. Tully and T.E. Madey, eds., Springer Series in Chemical Physics, Vol. 24 (Springer-Verlag, Heidelberg, 1983).

[2] D. Menzel, J. Vac. Sci. Technol. 20 (1982) 538.

[3] T.E. Madey, in Inelastic Particle-Surface Collisions, Springer Series in Chemical Physics 17, eds., E. Taglauer and W. Heiland (Springer-Verlag, Berlin, 1981) p. 80.

[4] H. Niehus, Applic. Surface Sci. 13 (1982) 292.

[5] C.G. Pantano and T.E. Madey, Applic. Surface Sci. 7 (1981) 115.

[6] T.E. Madey and J.T. Yates, Jr., Surface Sci. 63 (1977) 203.

[7] D. Menzel, in Interactions on Metal Surfaces, ed. R. Gomer (Springer-Verlag, Berlin, 1975) p. 124; Surf. Sci. 47 (1975) 370.

[8] D. Lichtman and Y. Shapira, in Chemistry and Physics of Solid Surfaces, ed. R. Vanselow (CRC, Boca Raton, 1978) p. 397.

[9] T.E. Madey and R. Stockbauer, in R.L. Park and M.G. Lagally, eds., Experimental Methods in Surface Science (in press).

[10] H. Niehus, Surface Sci. 78 (1978) 667; 80 (1979) 245.

[11] P. Feulner, R. Treichler, and D. Menzel, Phys. Rev. B24 (1981) 7427.

[12] D.E. Eastman, J.J. Donelon, N.C. Hien, and F.J. Himpsel, J. Nucl. Instr. Methods 172 (1980) 327.

[13] J.F. van der Veen, F.J. Himpsel, D.E. Eastman, and P. Heimann, Solid State Comm. 36 (1980) 99.

[14] T.E. Madey, R. Stockbauer, J.F. van der Veen, and D.E. Eastman, Phys. Rev. Lett. 45 (1980) 187.

[15] M. Knotek, V.O. Jones, and V. Rehn, Phys. Rev. Lett. 43 (1979) 300.

[16] D.M. Hanson, R. Stockbauer and T.E. Madey, Phys. Rev. B24 (1981) 5513.

[17] M.M. Traum and D.P. Woodruff, J. Vac. Sci. Technol. 17 (1980) 1202.

[18] T.E. Madey, Surface Sci. 79 (1979) 575.

[19] F.P. Netzer and T.E. Madey, J. Chem. Phys. 76 (1982) 710.

[20] See T.E. Madey, F.P. Netzer, J.E. Houston, D.M. Hanson and R. Stockbauer in Ref. 1, op. cit., p. 120.

[21] W.L. Clinton, Surf. Sci. 112 (1981) L791.

[22] E. Preuss, Surface Sci. 94 (1980) 249 and references therein.

[23] F.P. Netzer and T.E. Madey, Phys. Rev. Lett. 47 (1981) 928.

[24] T.E. Madey and F.P. Netzer, Surface Sci. 117 (1980) 549.

[25] F.P. Netzer and T.E. Madey, Surface Sci. 119 (1982) 422; Chem. Phys. Lett. 88 (1982) 315.

[26] C. Benndorf and T.E. Madey, Surface Sci. (to be published).

[27] J.K. Sass, K. Kretzschmar, and S. Holloway, Vacuum 31 (1980) 483.

[28] D.L. Doering, S. Semancik and T.E. Madey, Surface Sci., to be published.

[29] D.L. Doering and T.E. Madey, Surface Sci. 123 (1982) 305.

[30] E.D. Williams and D.L. Doering, J. Vac. Sci. Technol., (in press).

[31] H. Kistenmacher, H. Popkie, and E. Clementi, J. Chem. Phys. 61 (1974) 799.

[32] M.L. Knotek, in Ref. 1, op. cit., p. 139.

[33] M.L. Knotek and P.J. Feibelman, Phys. Rev. Lett. 40 (1978) 964; Surface Sci. 90 (1979) 78.

[34] E. Bertel, R. Stockbauer and T.E. Madey, J. Vac. Sci. Technol., (in press).

[35] D.M. Hanson, R. Stockbauer and T.E. Madey, Phys. Rev. B24 (1981) 5513.

[36] P.A. Redhead, Can. J. Phys. 42 (1964) 886.

[37] D. Menzel and R. Gomer, J. Chem. Phys. 41 (1964) 3311.

[38] See D.E. Ramaker in Ref. 1, op. cit., p. 70.

[39] T.E. Madey, R. Stockbauer, S.A. Flodstrom, J.F. van der Veen, F.J. Himpsel and D.E. Eastman, Phys. Rev. B23 (1981) 6847.

[40] D.E. Ramaker, J. Chem. Phys., (in press).

[41] R. Jaeger, J. Stohr, R. Treichler and K. Baberschke, Phys. Rev. Lett. 47 (1981) 1300.

[42] D.M. Hanson, R. Stockbauer and T.E. Madey, J. Chem. Phys. 77 (1982) 1569.

[43] E. Bertel, R. Stockbauer and T.E. Madey, J. Chem. Phys. 76 (1982) 5639.

[44] M.D. Burrows, S.R. Ryan, W.E. Lamb, Jr., and L.C. McIntyre, Jr., J. Chem. Phys. 71 (1979) 4931.

[45] D.E. Ramaker, Chemical Physics (in press).

Figure Captions

Fig. 1. Schematic bonding configurations for adsorbed H_2O and adsorbed CO, showing relationship between surface bond angles and ion desorption angles in ESDIAD.

Fig. 2. LEED and ESDIAD patterns for H_2O adsorbed on clean and oxygen-dosed Ni(111) at 80 K. (a) LEED pattern from clean Ni(111) surface, electron energy V_e = 120 eV; (b) H^+ ESDIAD pattern for a fractional monolayer of H_2O on clean Ni(111), V_e = 300 eV (the darker region around 4 o'clock is due to a low-gain region of the detector); (c) H^+ ESDIAD pattern from H_2O adsorbed on oxygen-predosed Ni(111), V_e = 300 eV. The arrows point in the direction of [$\bar{1}\bar{1}$2] azimuths (From Ref. 24, with permission).

Fig. 3. Schematic bonding model for O + H_2O on Ni(111); single O atoms are shown influencing the ordering of one, two or three H_2O molecules. (From Ref. 24, with permission).

Fig. 4 H^+ ESDIAD patterns for H_2O adsorbed on clean and Na-dosed Ru(001) surface. (a) H^+ ESDIAD for a fractional monolayer of H_2O adsorbed on clean Ru(001) at 80 K; (b) H^+ ESDIAD for H_2O adsorbed onto a low coverage of Na ($\Theta_{Na} \lesssim 0.1$) at 80 K; (c) after annealing surface of (b) to 210 K.

Fig. 5. (a) Schematic bonding model for H_2O + Na on Ru(001); a single adsorbed Na atom is shown influencing three H_2O molecules. (b) Schematic hexagonal H^+ ESDIAD pattern. Three beams are due to H^+ emission from H_2O molecules as shown in (a); three beams are due to a second domain of H_2O + Na, rotated 60° (see text).

Fig. 6. Schematic bonding models (side views) of adsorbed H_2O molecules interacting with electronegative adsorbate (oxygen) and electropositive adsorbate (sodium).

Fig. 7. Bottom curve: PSD O^+ yield vs. photon energy following an exposure of 8 X 10^{-6} Torr sec. of O_2 onto a Ti(001) surface at 300 K. Upper curve: constant final state (CFS) secondary electron yield spectrum for clean Ti(001) vs. photon energy. The form of the CFS spectrum is similar to the photoabsorption coefficient for Ti. (From Ref. 16, with permission).

Fig. 8. Comparison of PSD O^+ ion yield for CO on Ru(001) with secondary electron yield. (a) O^+ PSD yield vs. photon energy; (b) constant final state secondary electron yield for Ru(001). This comparison indicates that PSD of O^+ is not correlated with production of 4p core holes in Ru. (From Ref. 39, with permission).

Fig. 9. A compilation of ESD ion yields in the core region for a number of molecules adsorbed on surfaces; adsorbate core thresholds are indicated. Intensities are not to the same scale, but to the same zero. Note the distinctly delayed onsets for N1s and O1s, apparently due to the role of shake-up processes (two hole excitations) in ion formation. (From Ref. 11, with permission).

Fig. 10. H^+ PSD ion yields vs. photon energy for thin films ($\gtrsim$ 4 monolayers) of H_2O and CH_3OH condensed onto metal substrates at 80 K.

Fig. 11. Build-up of ESD ion signals as a function of exposure during adsorption of cyclohexane, C_6H_{12}, on a clean Cu(100) surface at 80 K. The high mass fragments ($C_1H_x^+$,....$C_6H_x^+$) only appear when multilayers of C_6H_{12} are formed, but H^+ appears from fractional monolayers. (1L = 1 X 10^{-6} Torr sec).

Fig. 12. Time-of-Flight mass spectra from electron stimulated desorption of condensed films of CH_3OH and C_6H_{12} at 80 K; (a) cyclohexane, taken at an ion kinetic energy of 1.5 eV; (b) methanol, taken at 3.8 eV ion kinetic energy.

Fig. 7. Bottom curve: PSD O^+ yield vs. photon energy following an exposure of 8 X 10^{-6} Torr sec. of O_2 onto a Ti(001) surface at 300 K. Upper curve: constant final state (CFS) secondary electron yield spectrum for clean Ti(001) vs. photon energy. The form of the CFS spectrum is similar to the photoabsorption coefficient for Ti. (From Ref. 16, with permission).

Fig. 8. Comparison of PSD O^+ ion yield for CO on Ru(001) with secondary electron yield. (a) O^+ PSD yield vs. photon energy; (b) constant final state secondary electron yield for Ru(001). This comparison indicates that PSD of O^+ is not correlated with production of 4p core holes in Ru. (From Ref. 39, with permission).

Fig. 9. A compilation of ESD ion yields in the core region for a number of molecules adsorbed on surfaces; adsorbate core thresholds are indicated. Intensities are not to the same scale, but to the same zero. Note the distinctly delayed onsets for N1s and O1s, apparently due to the role of shake-up processes (two hole excitations) in ion formation. (From Ref. 11, with permission).

Fig. 10. H^+ PSD ion yields vs. photon energy for thin films ($\gtrsim$ 4 monolayers) of H_2O and CH_3OH condensed onto metal substrates at 80 K.

Fig. 11. Build-up of ESD ion signals as a function of exposure during adsorption of cyclohexane, C_6H_{12}, on a clean Cu(100) surface at 80 K. The high mass fragments with a kinetic energy of $\sim$ 2 eV ($C_1H_x^+$,....$C_6H_x^+$) only appear when multilayers of C_6H_{12} are formed, but H^+ with a kinetic energy of $\sim$ 4 eV appears from fractional monolayers. (1L = 1 X 10^{-6} Torr sec).

Fig. 12. Time-of-Flight mass spectra from electron stimulated desorption of condensed films of CH_3OH and C_6H_{12} at 80 K; (a) cyclohexane, taken at an ion kinetic energy of 1.5 eV; (b) methanol, taken at 3.8 eV ion kinetic energy.

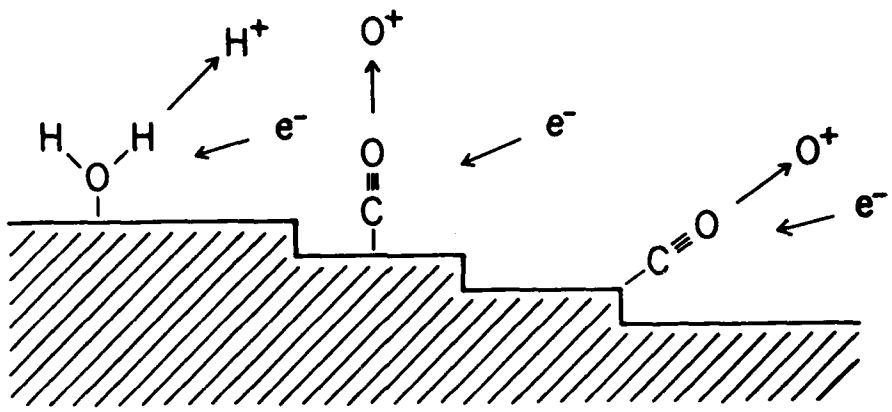

Fig. 1

Adsorption of H_2O on Clean and Oxygen - Dosed Ni (111)

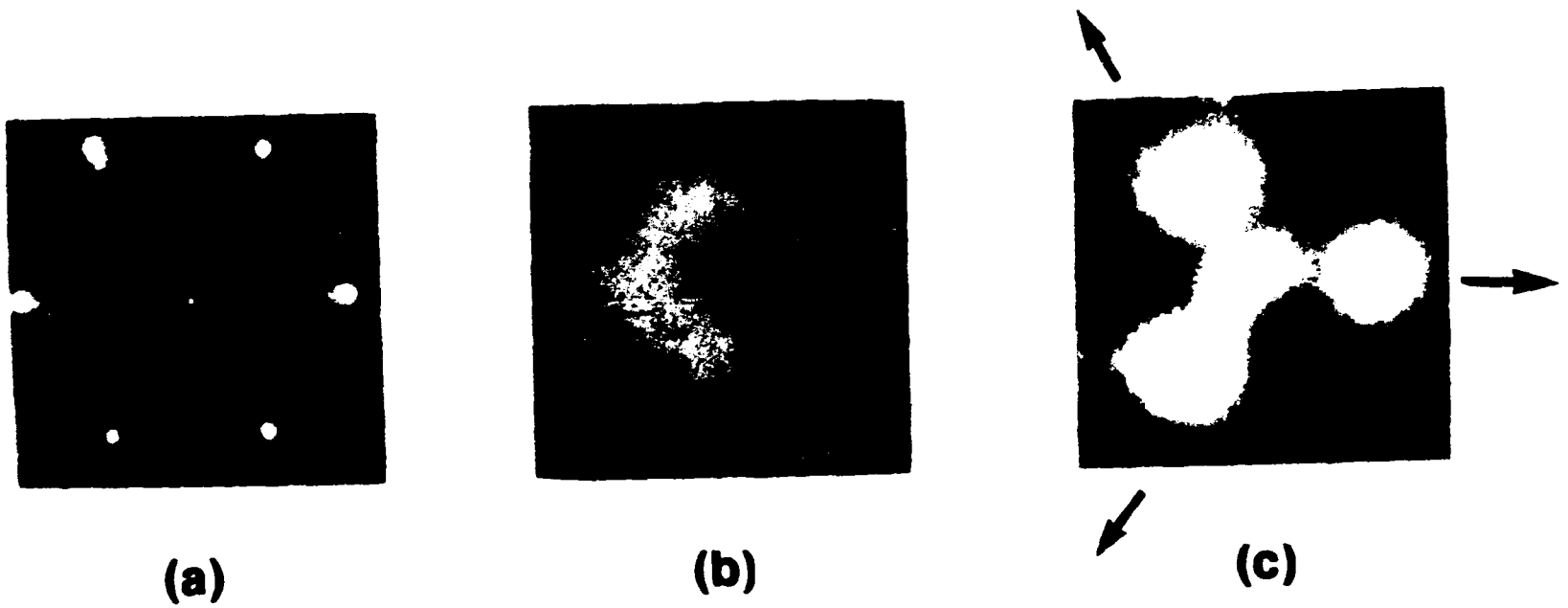

(a) (b) (c)

Fig. 2

Model for Orientation of H_2O

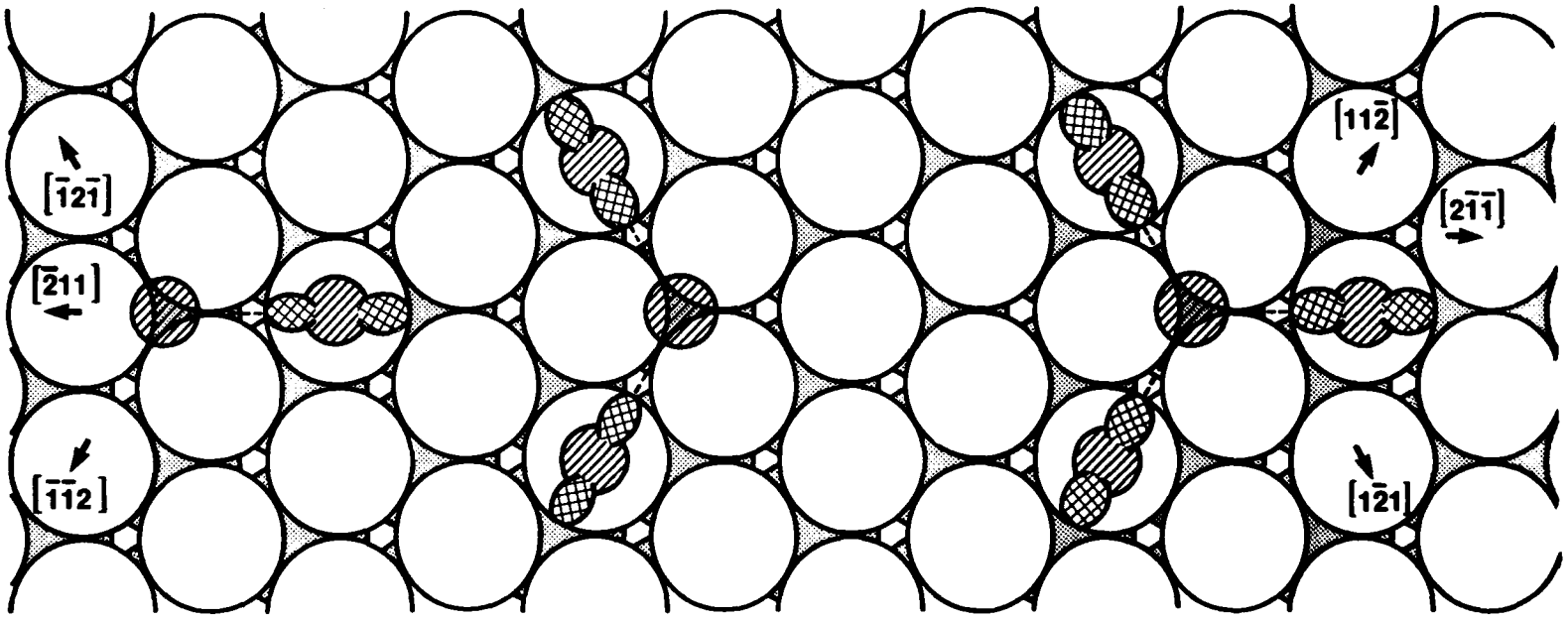

Fig. 3

ESDIAD FROM WATER ON SODIUM-PREDOSED RU(001)

($\theta_{H_2O} \approx 0.1$)

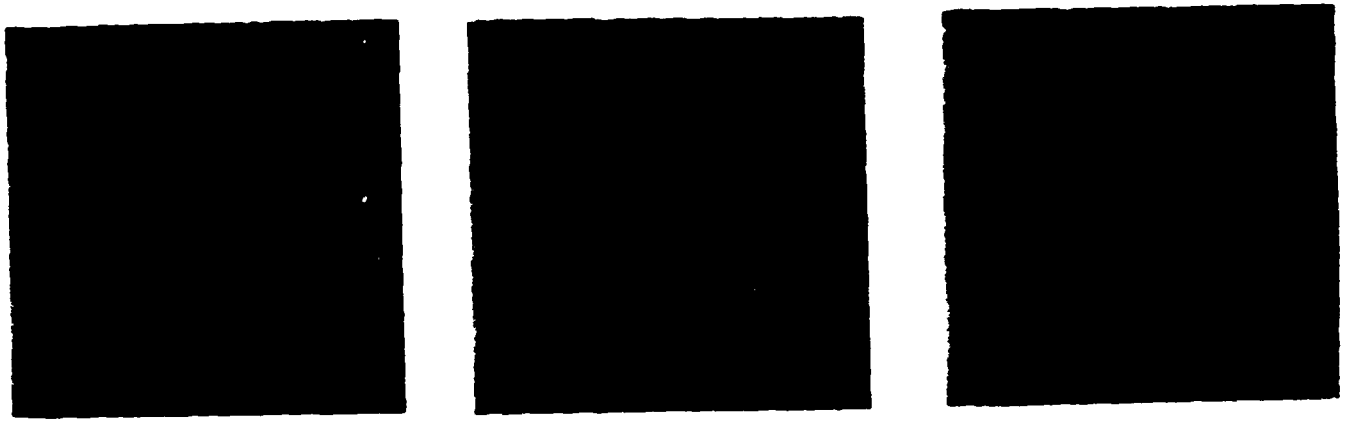

$\theta_{Na} = 0.0$ $\theta_{Na} \approx 0.1$

T = 80K T = 80K Annealed to 210K

Fig. 4

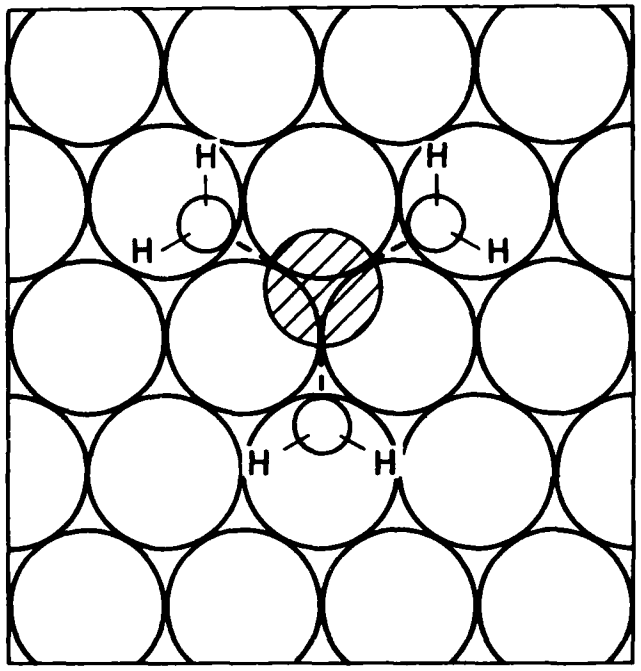

(a)

MODEL OF H_2O + Na
ON Ru (001)

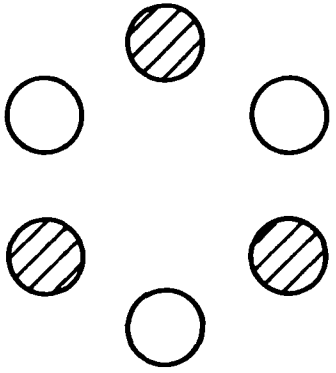

(b)

SCHEMATIC
H^+ ESDIAD PATTERN

Fig. 5

Interaction of H_2O with Adsorbed Atoms

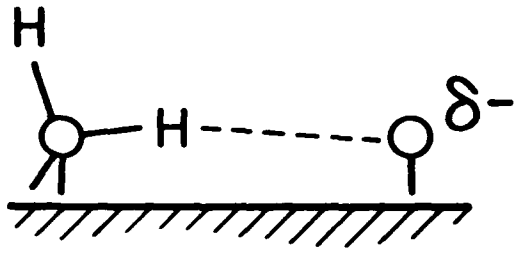

H_2O + oxygen

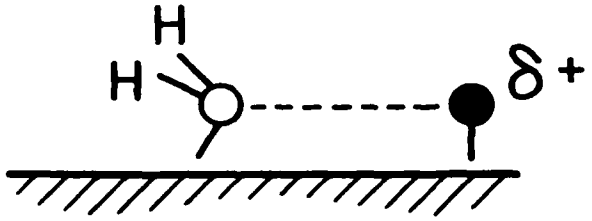

H_2O + sodium

Fig. 6

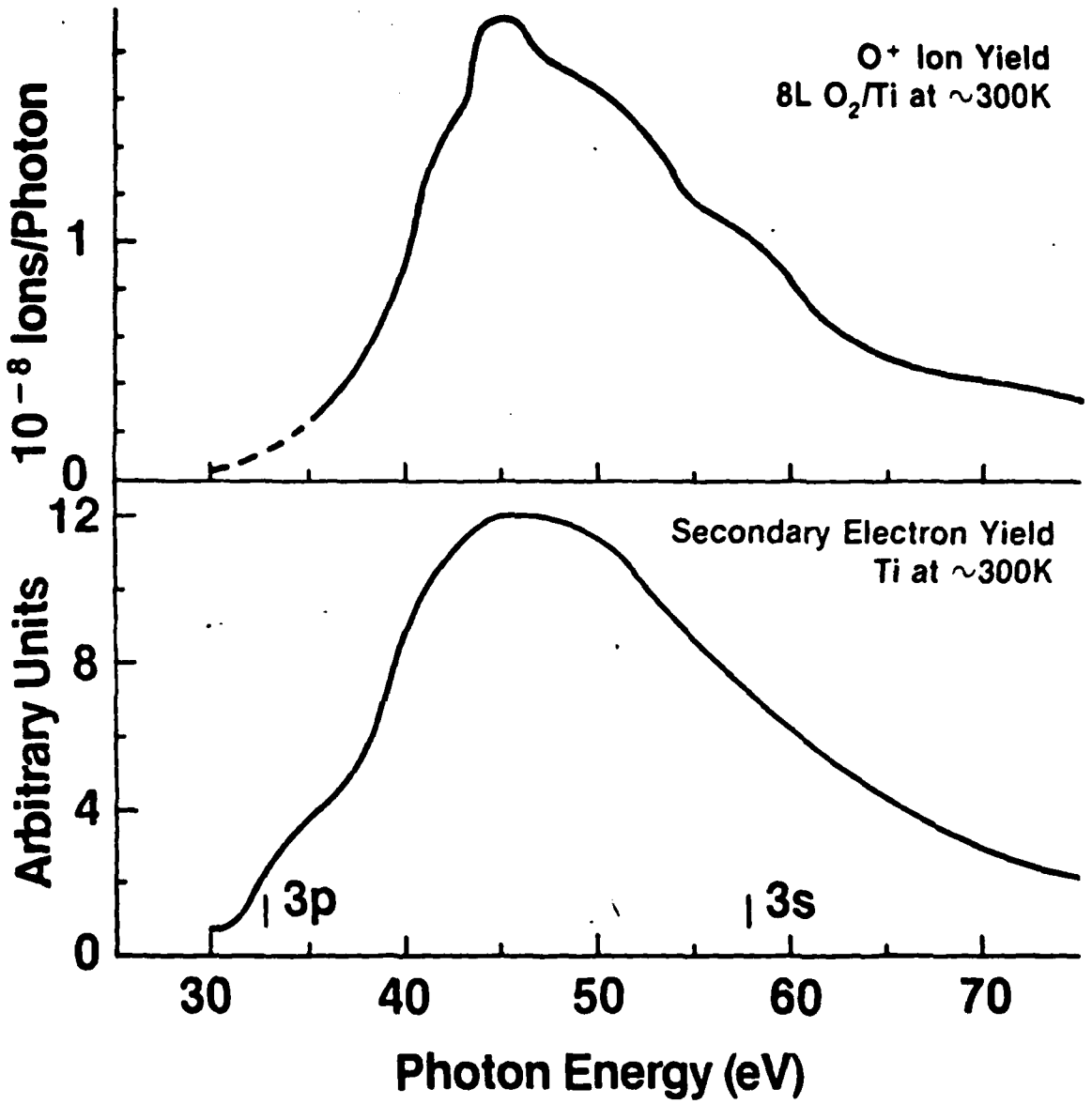
O+ Ion Yield
8L O2/Ti at ~300K
10−8 Ions/Photon
1
0
Secondary Electron Yield
Ti at ~300K
Arbitrary Units
12
8
4
0
3p
3s
30
40
50
60
70
Photon Energy (eV)

Fig. 7

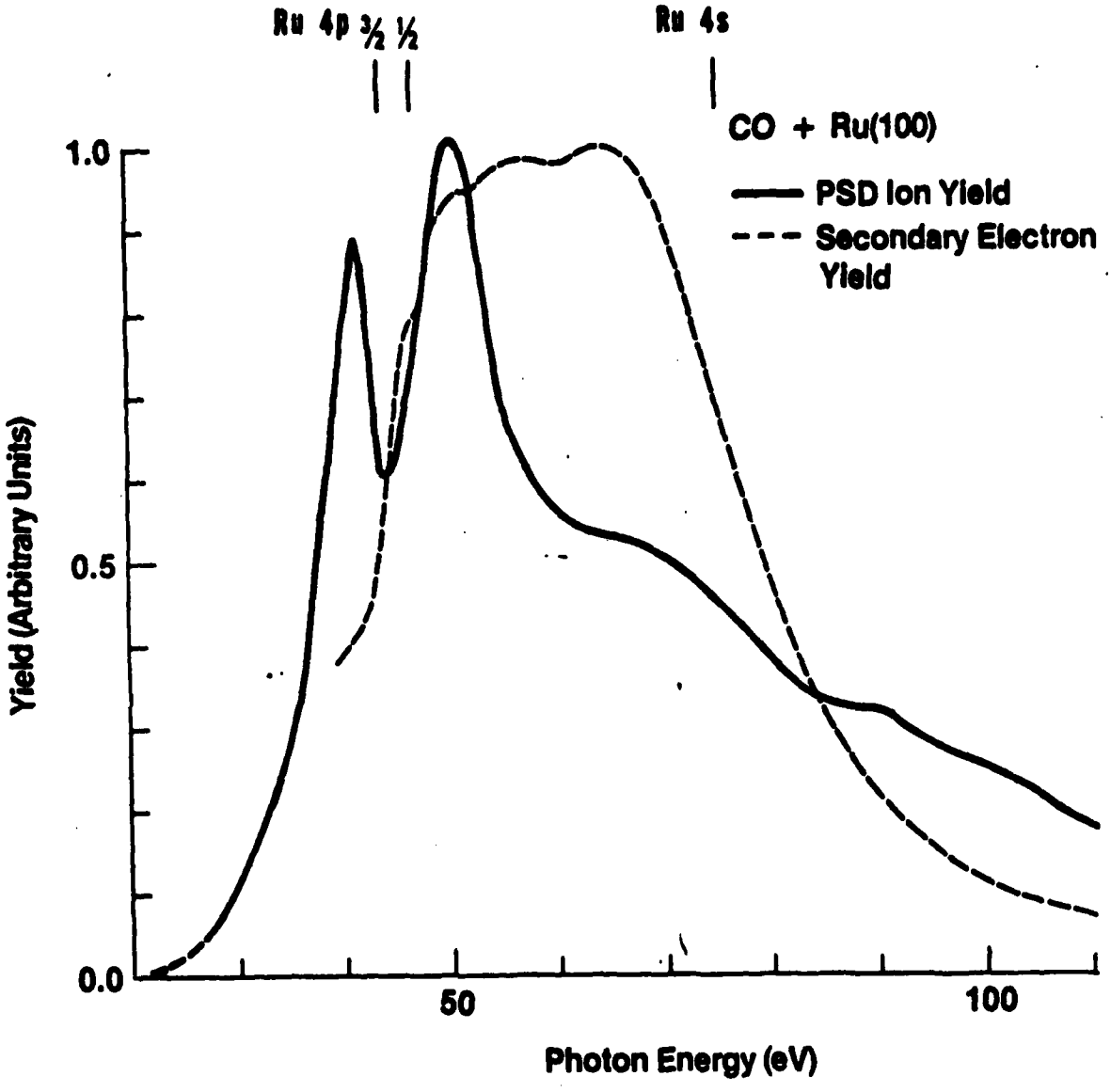
Ru 4p 3/2 1/2
Ru 4s
CO + Ru(100)
PSD Ion Yield
Secondary Electron Yield
1.0
0.5
0.0
Yield (Arbitrary Units)
50
100
Photon Energy (eV)

Fig. 8

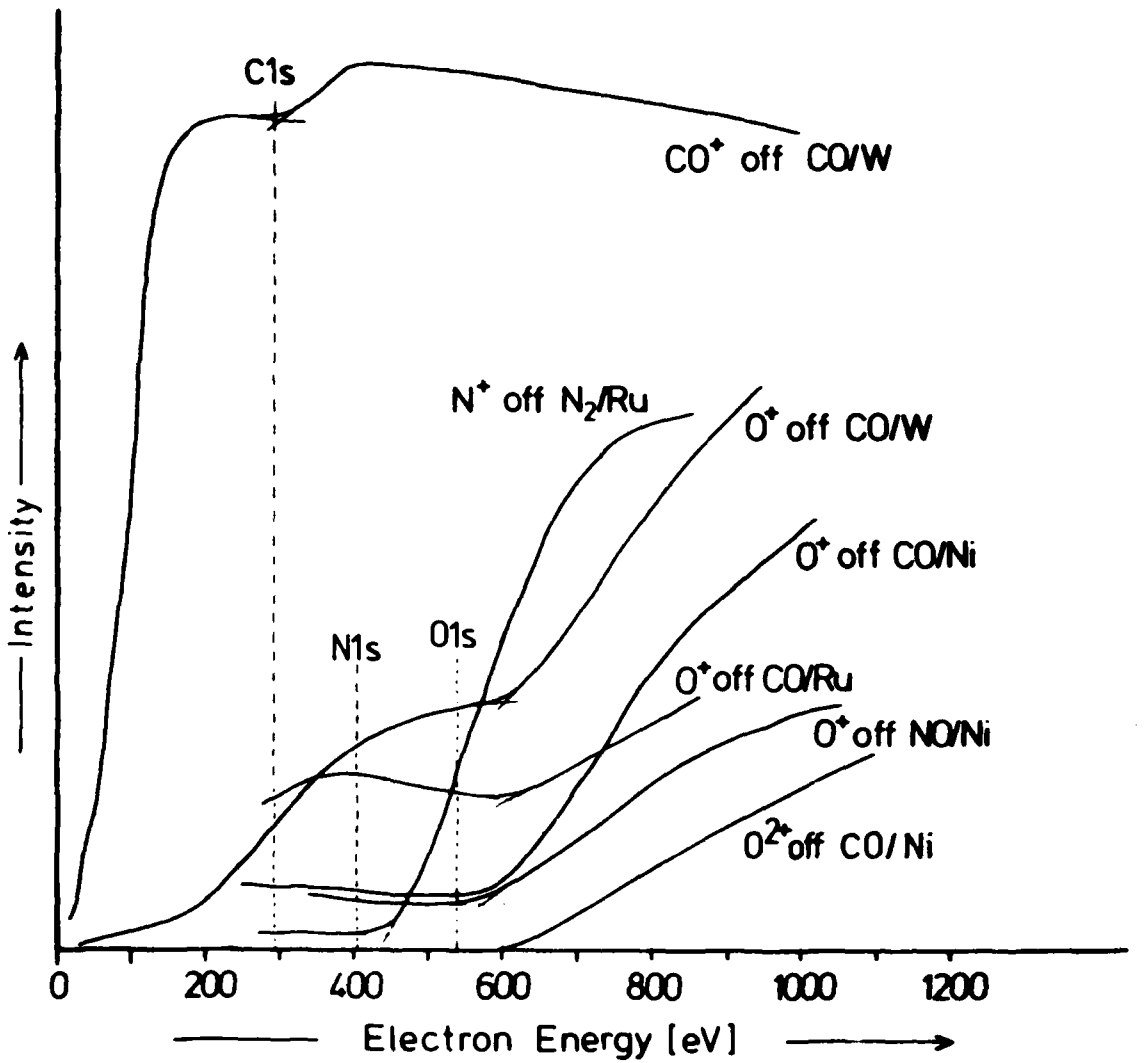
C1s
CO⁺ off CO/W
N⁺ off N₂/Ru
O⁺ off CO/W
O⁺ off CO/Ni
N1s
O1s
O⁺off CO/Ru
O⁺off NO/Ni
O²⁺off CO/Ni
Intensity
0
200
400
600
800
1000
1200
Electron Energy [eV]

Fig. 9

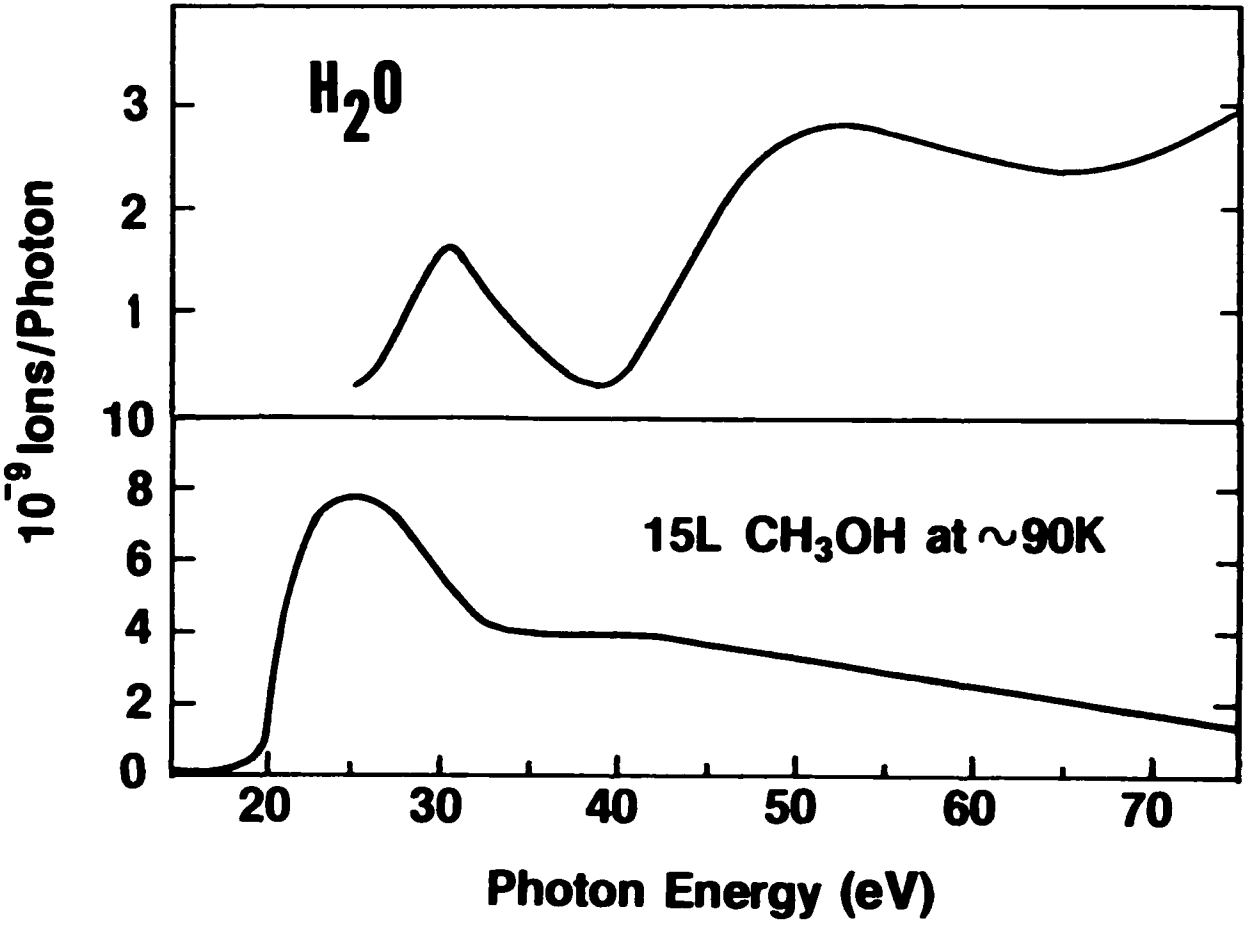
H_2O
3
2
1
10
8
6
4
2
0
10^{-9} Ions/Photon
15L CH_3OH at ~90K
20
30
40
50
60
70
Photon Energy (eV)

Fig. 10

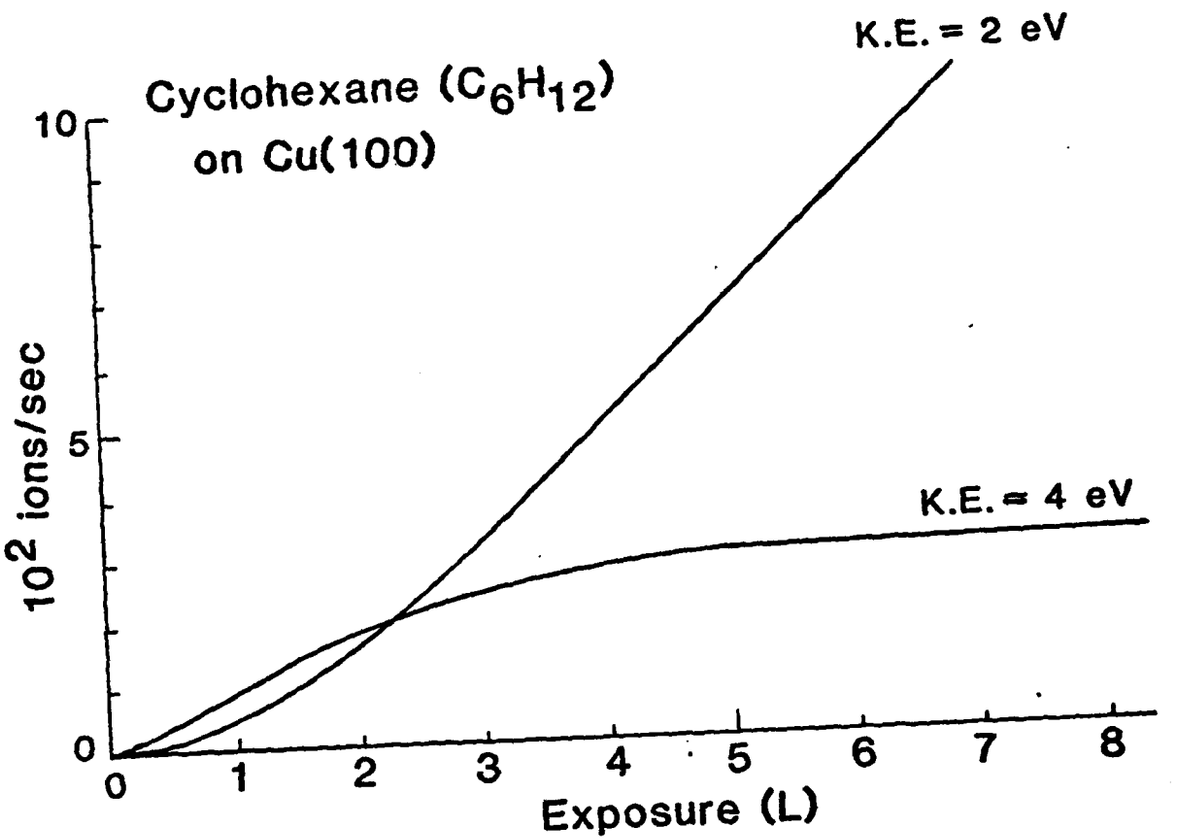
Cyclohexane (C_6H_{12})
on Cu(100)
K.E. = 2 eV
K.E. = 4 eV
10^2 ions/sec
10
5
0
0
1
2
3
4
5
6
7
8
Exposure (L)

Fig. 11

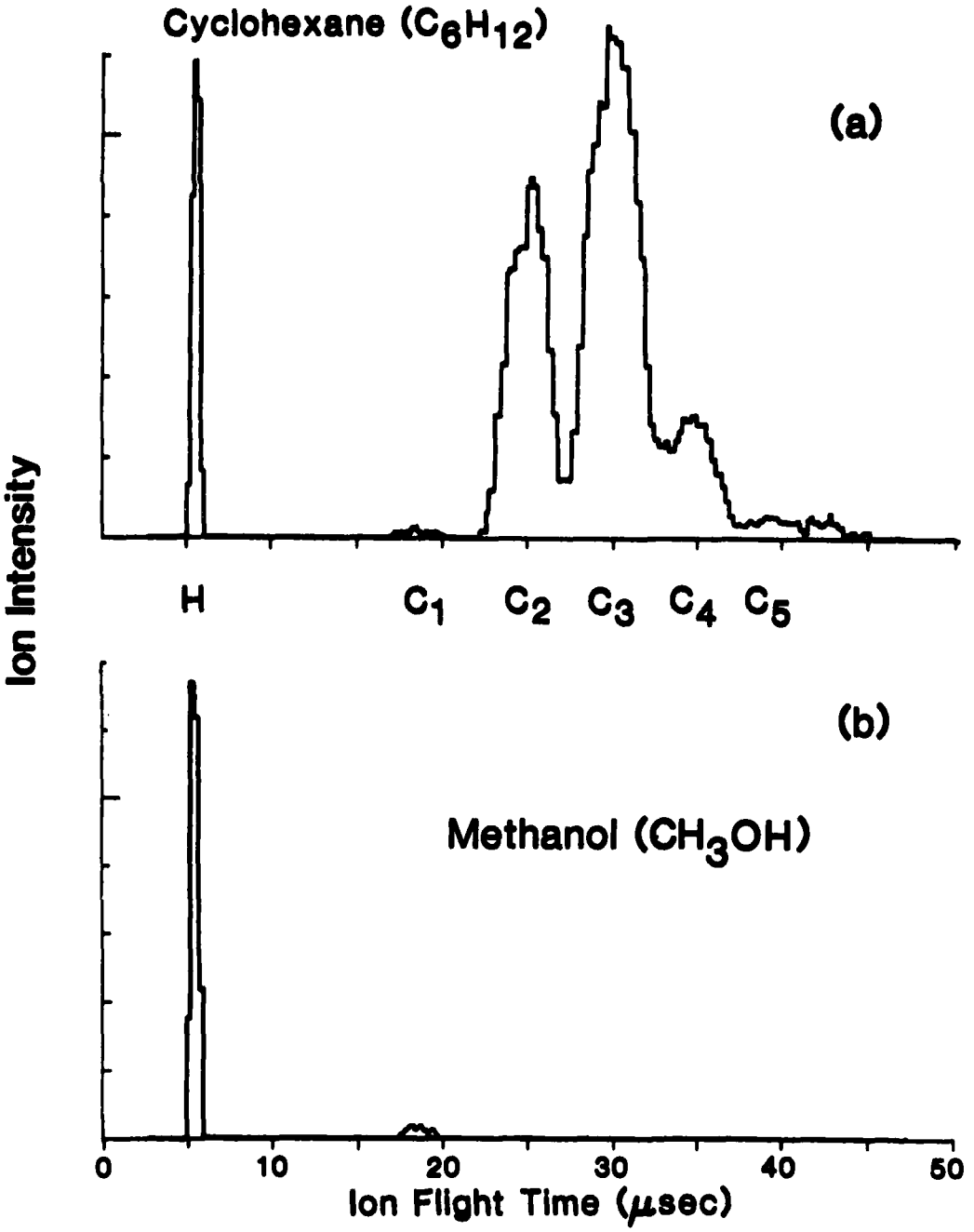
Cyclohexane (C_6H_{12})
(a)
Ion Intensity
H
C_1
C_2
C_3
C_4
C_5
(b)
Methanol (CH_3OH)
0
10
20
30
40
50
Ion Flight Time (μsec)

Fig. 12